Accurate analysis of 10 nm emission zone features in OLED

L. Paniagua Rodríguez* **, D. Michaelis*, C. Pflumm***, W. Brütting**, N. Danz *

*Fraunhofer Institute of Applied Optics and Precision Engineering (IOF), Jena
**Institute of Physics, University of Augsburg, Augsburg
***Merck Electronics KGaA, Darmstadt

mailto: luis.paniagua.rodriguez@iof.fraunhofer.de

Optimizing the emission zone (EMZ) is crucial for enhancing OLED efficiency and lifespan. The thin active layer (typically on the order of 10 nm) complicates measuring EMZ details from radiation patterns. By using a polynomial description reduced to two parameters, we can estimate resolution limits, track shifts, and define optimization targets.Exemplarily, this new 2D visualization of EMZs is applied to current-dependent EMZ changes of a mixed host OLED.

1 Introduction

For the development of highly efficient Organic Light-Emitting Diodes (OLEDs) [1][2][3] it is essential to control the distribution of light generation inside the OLED's emissive layer (EML). Therefore, the precise analysis of such emission zone profiles (EMZ) is of great importance. In this paper, we show which emission zones can be reliably calculated back from the interference patterns of optical OLED emissions [4] and how these emission zones of different OLEDs can be clearly visualised and compared.

2 Experimental Determination of an OLED's EMZ

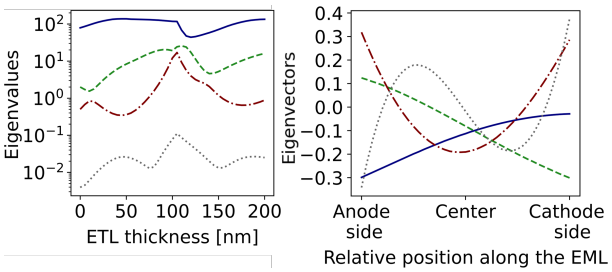

Fig. 1 *Left: eigenvalues of $\hat{M}(\lambda_k, \theta_k, \xi_i)$ dependent on ETL thickness, obtained using the SVD method. Right: associated eigenvectors for an ETL thickness of 120 nm.*

The OLED's far-field emission pattern is the linear superposition of the emission patterns of all emitters at every position ξ_i within the EML. A linear matrix equation can therefore be used for modelling, which converts the EMZ, $p(\xi_i)$, into the angular (θ_k) and wavelength (λ_k) dependent far-field emission pattern, $I(\lambda_k, \theta_k)$:

$$I(\lambda_k, \theta_k) = \hat{M}(\lambda_k, \theta_k, \xi_i) \cdot p(\xi_i). \qquad (1)$$

In a typical bottom-emitting OLED stack, interference effects can be adjusted by varying the thickness of the electron transport layer (ETL), which is located between the reflective cathode and the emissive layer.

If the eigenvalues of the matrix $\hat{M}(\lambda_k, \theta_k, \xi_i)$ are analyzed using Singular Value Decomposition (SVD) as a function of the ETL thickness, it can be seen that the maximum information for EMZ retrieval is obtained for far-field patterns with a destructive interference behavior. For the specific OLED stack used here, this occurs at ETL thicknesses around 120 nm, where the upper three eigenvalues are very close to each other, while all remaining eigenvalues are several orders of magnitude smaller (see Fig. 1 left). The three right-singular vectors associated to these eigenvalues form the basis functions for the measurable/analyzable EMZs (see Fig. 1 right). Their exact shapes depend on the specific OLED stack but they are always very closely related to the Legendre polynomials (see e.g. polynomial shapes with typical number of zeros). Therefore, with negligible loss of accuracy the measurable EMZs can also be represented as a linear combination of the first three Legendre polynomials:

$$P_0(x) = 1; \quad P_1(x) = x; \quad P_2(x) = \frac{1}{2}(3x^2 - 1). \qquad (2)$$

After scaling the EML to the normalized interval x $\in$ [-1,1] the measurable EMZs read as:

$$EMZ(x) \cong P_0(x) + p_1 P_1(x) + p_2 P_2(x). \qquad (3)$$

The coefficient of the polynomial $P_0(x)$ is eliminated through integral normalization as the shape of the relevant interference pattern does not depend on the total number of photons generated. The experimentally accessible EMZ distribuion is described by the only two parameters from Eq. 3, p_1 and p_2. This allows any EMZ to be mapped to a single point in the two-dimensional p_1-p_2 plane (see Fig. 2). The p_1-coordinate describes the asymmetry of the EMZ relative to the EML's center positions with large negative values indicating EMZs shifted towards the anode side and large positive values

DGaO Proceedings 2024 – http://www.dgao-proceedings.de – ISSN: 1614-8436 – urn:nbn:de:0287-2024-A022-0
submitted: 02.08.2024 – published: 12.08.2024

indicating shifts towards the cathode side. The p_2-coordinate accounts for the symmetric variations in the EMZ. When considering only positive EMZ contributions (i.e., $EMZ(x) \geq 0$), the p_1 and p_2 values are confined to a droplet-shaped region delimited by the expressions shown in Fig. 2.

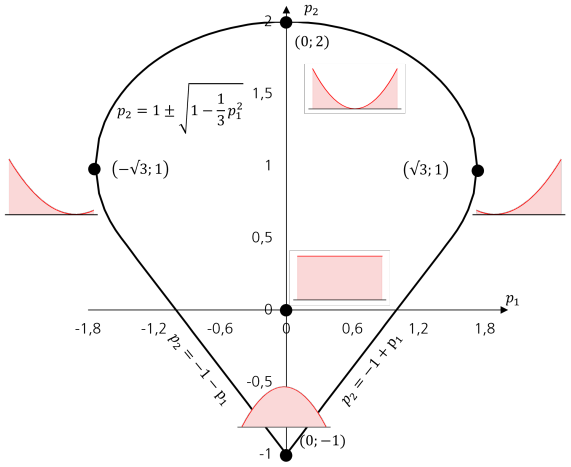

Fig. 2 *2D EMZ representation model. Area delimited by positive EMZ values form an inverse 'droplet' in the $p_1 - p_2$ plane. The plot includes boundary descriptions and examples of EMZs at the extremes and at the droplet's center.*

3 Practical example

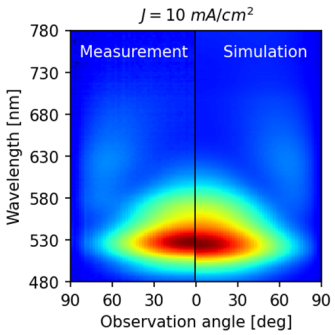

Fig. 3 *Far-field emission pattern measured at $J = 10mA/cm^2$, alongside its simulated counterpart.*

For practical analysis, OLED samples were prepared on a commercial substrate using thermal evaporation and subsequently treated with cleaning, annealing, and plasma processes. The OLED structure features a multi-layer configuration, including a 130 nm thick ETL and a mixed host EML composed of 66vol% electron-conducting material, 22vol% hole-conducting material, and 12vol% of a heteroleptic Iridium-based phosphor. Far-field emission patterns were measured with a goniometer, rotating the samples in 2° increments. Spectra were recorded in 2 nm steps at current densities ranging from 0.1 to 100 mA/cm² (see Fig. 3). The results of the EMZ analysis for these measurements are shown in Fig. 4. From this, we can see that as the current density increases, the EMZ shifts towards the left side of the droplet, indicating that within the stack, the EMZ is moving towards the hole-injection side.

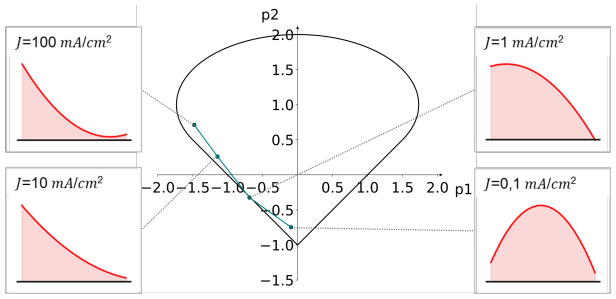

Fig. 4 *Fitting the experimental data yields current dependent EMZ that are illustrated by their distributions as well as their position in the p_1, p_2plane containing the droplet from Fig. 2 for convenience.*

4 Conclusion

Given that only three eigenvalues of the matrix containing the EMZ information can be resolved, and their associated system-specific eigenvectors can be universalized, we present an experimental characterization of the emission zone (EMZ) along the emissive layer of an OLED. This is achieved using a mathematical model based on Legendre polynomials and a 2D visualization to easily identify optimization targets. We applied our representation model to characterize the EMZ of the same device under different current densities, detecting and representing changes in the EMZ profile dependent on the applied current density.

References

[1] C. Tang and A. VanSlyke, "Organic electroluminescent diodes," Appl. Phys. Lett. **51**, 913–915 (1997).

[2] M. Pfeiffer, K. Leo, J. Zhou, J. Huang, M. Hofmann, and A. Werner, "Doped organic semiconductors: Physics and application in light emitting diodes," Org. Electron. **4 (2-3)**, 89–103 (2003).

[3] G. Hong, X. Gan, C. Leonhardt, Z. Zhang, J. Busch, and S. Bräse, "A Brief History of OLEDs - Emitter Development and Industry Milestones," Org. Electron. **4 (2-3)**, 89–103 (2003).

[4] N. Danz, M. Flämmich, D. Setz, B. Krummacher, D. Michaelis, and T. Dobbertin, "Detection of sub-10 nm emission profile features in organic light-emitting diodes using destructive interference," Optics Letters **37**, 4134–4136 (2012).